

TURBULENT MASS TRANSFER MECHANISM ACROSS A CONTAMINATED AIR-WATER INTERFACE

Yosuke Hasegawa & Nobuhide Kasagi
Department of Mechanical Engineering,
The University of Tokyo
Hongo 7-3-1, Bunkyo-ku, Tokyo, 113-8656, Japan
hasegawa@thtlab.t.u-tokyo.ac.jp, kasagi@thtlab.t.u-tokyo.ac.jp

ABSTRACT

Numerical simulation of high Schmidt number turbulent mass transfer across clean and contaminated air-water interfaces is carried out. At the clean interface, the local scalar flux is predicted fairly well from the surface divergence by applying the Chan and Scriven's stagnation flow model. With increasing the Marangoni number, however, the scalar flux is less correlated with the surface divergence and the gas transfer rate deteriorates drastically and eventually approaches the value on a solid wall. From an analysis of a one-dimensional advection-diffusion equation, it is shown that the scalar field near the interface is characterized by two time scales, *i.e.*, renewal and transient time scales, and the surface divergence contributes to the mass transfer only when the renewal time scale is longer than the transient time. The effective surface divergence is extracted from time-series data and found suitable for prediction of gas exchange at clean and slightly contaminated interfaces. In the case of the highly contaminated interface, in which the effective surface divergence is strongly damped, the mass transfer is essentially the same as that on a solid wall.

INTRODUCTION

It is well known that surface contamination retards gas exchange across a turbulent air-water interface. So far, numerous experiments have been carried out in wind-wave facilities and stirred vessels, *e.g.*, Jähne *et al.* (1987), Asher and Pankow (1986). In these studies, a similar transition in the gas exchange has been observed. Specifically, below a critical turbulence level, the gas transfer rate increases only slightly with the turbulence level and is proportional to $Sc^{-2/3}$ as in the case of a solid wall. Beyond the critical turbulence level, however, the gas transfer rate increases rapidly and the Schmidt number exponent changes from $-2/3$ to $-1/2$. The mechanism of the transition is not fully understood since the turbulence near the interface is affected by not only surface elasticity but also waves, which start to grow at the critical turbulence level.

Considering that most resistance to mass transfer resides in a very thin concentration boundary layer near the interface, understanding the transport mechanism inside the viscous sublayer is particularly important. Chan and Scriven (1970) first shed light on a critical role of irrotational stagnation flow in the mass transfer across a perfectly free liquid surface. After that, many experimental and theoretical researches, *e.g.*, McCready *et al.* (1986), Banerjee *et al.* (2004), supported that the total gas transfer rate is related to the intensity of surface divergence. However, the quantitative relationship between the local scalar flux and the surface divergence at a turbulent interface has not been investigated in detail, which is vital to assess the existing models.

In the present research, we focus on the interaction of turbulence with an elastic surface and its effects on the interfacial mass transfer at high Schmidt numbers. Particular attention is paid to the response of local scalar flux to the surface divergence in order to understand the transition mechanism in the mass transfer across a contaminated interface.

NUMERICAL PROCEDURES

Numerical conditions

In this study, a countercurrent air-water flow driven by constant pressure gradient is considered as shown in Fig. 1. The Reynolds numbers based on the interfacial friction velocity u_τ and the depth δ are set to be $Re_{\tau L} = Re_{\tau G} = 150$, which approximately corresponds to an air-water flow at a wind speed of 2 m/s at $y_G = \delta$ and δ of 4 cm under the standard condition. The density ratio of liquid and gas is $\rho_L / \rho_G = 841$. The Schmidt number is changed from 1.0 to 100 on the liquid side, while kept constant $Sc_G = 1.0$ on the gas side. The horizontal dimensions of a computational domain are $2.5\pi\delta$ and $\pi\delta$ in the streamwise and spanwise directions, respectively. A periodic boundary condition is employed for the horizontal directions, while a free-slip condition for outer boundaries so as to minimize their effects.

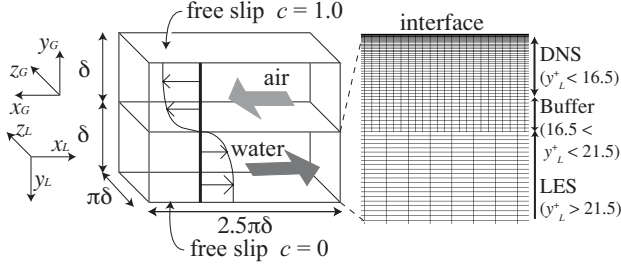


Figure 1: Computational domain and grid system in the hybrid DNS/LES scheme.

Table 1: Numbers of modes and grid points, and grid spacings in the shear unit.

		Region	$k_x, k_y \text{ or } N_y, k_z$	Δx_L^+	Δy_L^+	Δz_L^+
Velocity	DNS	$0 < y_L^+ < 150$	64, 128, 64	18.4	0.002 ~ 0.38	7.2
Scalar:	DNS	$0 < y_L^+ < 11.3$	192, 35, 192	6.1	0.01 ~ 0.62	2.4
Hybrid	Buffer	$11.3 < y_L^+ < 21.6$	192, 13, 192	6.1	0.66 ~ 0.85	2.4
DNS/LES	LES	$21.6 < y_L^+ < 150$	64, 144, 64	18.4	0.86 ~ 1.23	7.2

The governing equations are the incompressible Navier-Stokes, the continuity and the scalar transport equations. DNS is applied for the velocity and scalar fields at the low Schmidt number of $Sc_L = 1.0$ by using a pseudo-spectral method. Numbers of modes and grid spacings are listed in Table 1.

For the high Schmidt number of $Sc_L = 100$, a hybrid DNS/LES Scheme is applied.

Hybrid DNS/LES scheme

In order to calculate the high Schmidt number scalar field at feasible computational cost, we proposed a hybrid DNS/LES scheme, in which DNS with high-resolution grids is employed within the near-surface region, while LES with relatively coarse grids for the outer layer (see, Fig. 1). For spatial discretization, spectral and finite volume methods are used in the horizontal and normal directions, respectively.

The computational domain in the liquid phase is divided into three regions, i.e., a DNS region ($0 < y_L^+ < 16.8$), a buffer region ($16.8 < y_L^+ < 21.5$) and a LES region ($y_L^+ > 21.5$). Depth of the DNS region is determined so that 95% of a concentration difference occurs in this region.

The scalar transport equation in the three regions is described as:

$$\frac{\partial c}{\partial t} + u_j \frac{\partial c}{\partial x_j} = \frac{1}{Re_\tau \cdot Sc} \frac{\partial^2 c}{\partial x_j \partial x_j} + \frac{\partial}{\partial x_j} \left(-A_c \frac{\partial \xi_j}{\partial x_j} \right) \quad (1)$$

Here, ξ_j is subgrid-scale scalar flux. In this study, the dynamic Smagorinsky model is used to close Eq. (1).

$$\xi_j = -C_s \Delta^2 |S_{ij}| \frac{\partial c}{\partial x_j} \quad (2)$$

In Eq. (1), A_c is a switch function from DNS ($A_c = 0$) to LES ($A_c = 1$). In the buffer region, A_c is gradually increased from 0 to 1 as going away from the interface.

Computation with finer grids and a deeper DNS region was also made in order to ensure that these effects on statistics in the DNS region were negligibly small.

Boundary conditions at a contaminated air-water interface

Since we focus on the effects of surface contamination on high Schmidt number mass transfer, the interface is assumed to be flat for simplicity. This is plausible for a contaminated interface, in which turbulence and capillary waves are drastically damped due to the Marangoni effect. The resultant boundary condition for the velocity field is the continuity of the velocity and shear stress in the horizontal directions.

$$u_{Lj} = u_{Gj} \quad (3)$$

$$\frac{1}{Re_{\tau L}} \frac{\partial u_{Lj}}{\partial x_2} = \frac{1}{Re_{\tau G}} \frac{\partial u_{Gj}}{\partial x_2} + \frac{Ma}{We} \frac{\partial \gamma}{\partial x_j} \quad (4)$$

Here, j is 1 or 3 and γ is the surfactant concentration. The Weber number We and the Marangoni number Ma are defined as $We = \rho_L u_{\tau L}^2 \delta / \sigma_0$ and $Ma = -(\gamma_0 / \sigma_0)(d\sigma / d\gamma)_0$, respectively. The subscript 0 represents evaluation at equilibrium and σ is the surface tension. Since the ratio of We to Ma is essential in Eq. (4), the Marangoni number is changed systematically as $Ma = 0$ (clean), 10^{-3} (Case 1), 10^{-2} (Case 2) and 10^{-1} (Case 3), while the Weber number is kept constant $We = 9.0 \cdot 10^{-3}$.

RESULTS

Velocity field

The mean velocity profiles relative to the interfacial velocity in the liquid phase are shown in Fig. 2. Data near a solid wall is also plotted for comparison. Although the logarithmic region with the same slope is observed, a gap exists between a clean interface and a solid wall. With increasing the Marangoni number, the thickness of the viscous sublayer is gradually increased and the profile converges to that near a solid wall.

The velocity fluctuations in the liquid phase are shown in Fig. 3. In contrast to the mean velocity, the streamwise and spanwise velocity fluctuations are almost unchanged, while only the normal velocity fluctuation is dumped drastically with increasing the Marangoni number. This indicates that the velocity field near a highly contaminated interface is essentially different from that near a solid wall.

In order to clarify the surfactant effects on the flow field, we decomposed the interfacial velocity vectors into irrotational and solenoidal components by applying Helmholtz's theorem (see, Fig. 4). The kinetic energy contained in the two components k_{IR} and k_{SL} are listed in Table 2. A distinctive feature of a contaminated interface is selective damping

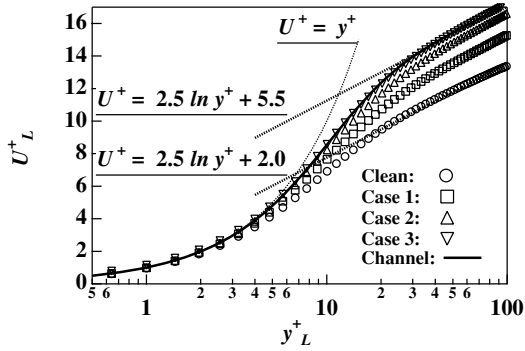


Figure 2: Mean velocity profiles in the liquid phase.

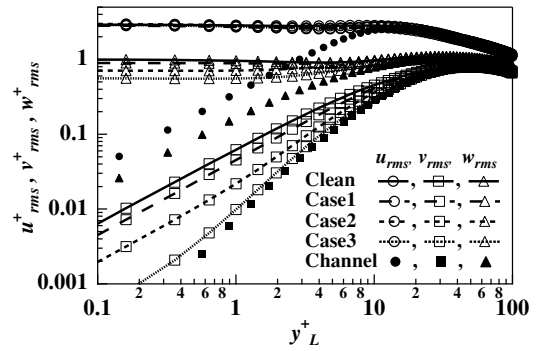


Figure 3: Velocity fluctuations in the liquid phase.

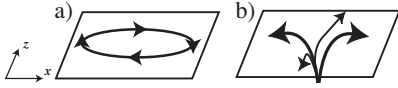


Figure 4: Decomposition of the interfacial velocity vector into a) solenoidal and b) irrotational components.

Table 2: Decomposition of the turbulent kinetic energy and gas transfer rates at contaminated interfaces.

	Ma	k_{Total}	k_{SL}	k_{IR}	$K^+_{Sc=1.0}$	$K^+_{Sc=100}$
Clean	0	9.2	7.8	1.37	$6.8 \cdot 10^{-2}$	$9.6 \cdot 10^{-3}$
Case 1	$1.0 \cdot 10^{-3}$	8.7	7.8	0.86	$5.9 \cdot 10^{-2}$	$5.2 \cdot 10^{-3}$
Case 2	$1.0 \cdot 10^{-2}$	7.4	7.0	0.36	$5.4 \cdot 10^{-2}$	$3.9 \cdot 10^{-3}$
Case 3	$1.0 \cdot 10^{-1}$	7.3	7.2	0.06	$5.1 \cdot 10^{-2}$	$3.6 \cdot 10^{-3}$

of the irrotational motion. Namely, the contaminated interface behaves like a no-slip boundary for the irrotational motion, while a free-slip boundary for the solenoidal motion. Although the irrotational motion constitutes a small fraction in the total kinetic energy, it holds a great significance in the interfacial mass transfer as shown below.

Scalar field

Gas transfer rate. Gas transfer rates at $Sc_L = 1.0$ and 100 are listed in Table 2. Surface contamination has a profound effect at the high Schmidt number, since the most resistance to mass transfer lies in a thinner layer at the top of the liquid. Specifically, the gas transfer rate is decreased by 60 % at $Sc_L = 100$, while only 25 % at $Sc_L = 1.0$.

According to recent experiments and numerical simulations, the gas transfer rate is well related to the intensity of surface divergence as:

$$K^+ = \frac{K}{u_{\tau L}} = \frac{\bar{q}}{\Delta C} \cong C \sqrt{\frac{\beta^+_{rms}}{Sc}} \quad (5)$$

Here, the surface divergence is defined as:

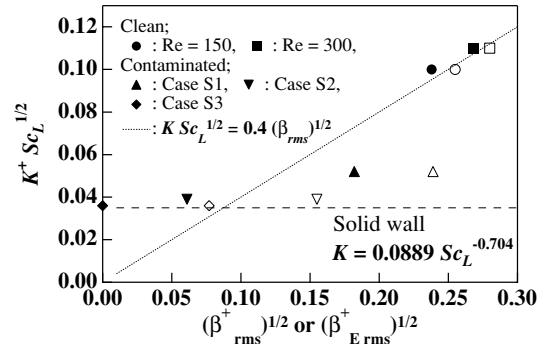


Figure 5: Gas transfer rates versus the surface divergence. Abscissa axis: open symbols; β_{rms} , solid symbols; $\beta_{E rms}$.

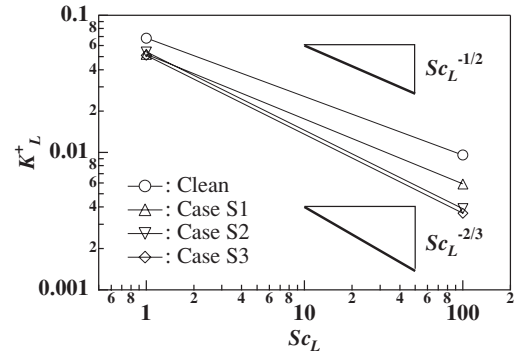


Figure 6: Gas transfer rates versus the Schmidt number.

$$\beta = \left(\frac{\partial u}{\partial x} + \frac{\partial w}{\partial z} \right) \Big|_{y=0} = - \frac{\partial v}{\partial y} \Big|_{y=0} \quad (6)$$

According to the existing data, the proportional constant C is about 0.4 for a sheared interface (Banerjee et al., 2004). In Fig. 5, the gas transfer rate at $Sc_L = 100$ is plotted as a function of the surface divergence with open symbols. At the clean interface, the present result shows good agreement with Eq. (5). With increasing the Marangoni number, however, the gas transfer rate is decreased drastically and converges

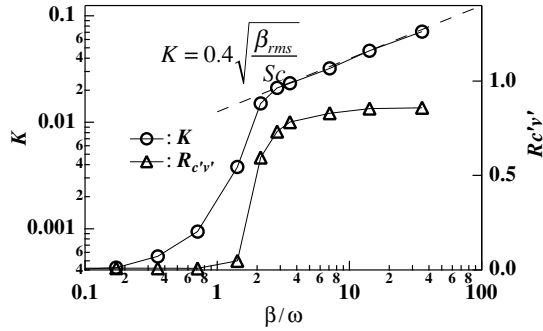


Figure 7: Gas transfer rates K and correlation coefficients $R_{c'v'}$ between the velocity and scalar fluctuations.

to that at a solid wall. The gas transfer rate versus the Schmidt number is plotted in Fig. 6. Although only two data points are available, it is observed that the Schmidt number exponent transits from $-1/2$ at clean and slightly contaminated interfaces to $-2/3$ at highly contaminated interfaces.

These results suggest that the contribution of the surface divergence to the mass transfer becomes less significant at the highly contaminated interface and the transport mechanism switches to that at a solid wall.

One-dimensional gas transfer model. In order to clarify the relationship between the scalar flux and the surface divergence, one-dimensional advection-diffusion equation becomes useful. Chan and Scriven (1970) considered mass transfer in an irrotational stagnation flow and showed that the transport equation reduces without approximation to:

$$\frac{\partial c}{\partial t} - \beta(t)y \frac{\partial c}{\partial y} = \frac{1}{Sc} \frac{\partial^2 c}{\partial y^2} \quad (7)$$

Here, all variables are non-dimensionalized by the shear units. By introducing a new coordinate system $Y = y\sqrt{Sc_L}$, the Schmidt number disappears from Eq. (7). If we represents the fluctuating surface divergence as $\beta(t) = \beta \cos(\omega \cdot t)$, important parameters characterizing the properties of the solution are β and ω . The inverses of the two parameters correspond to different time scales as discussed below.

According to the Chan and Scriven's result for steady upwelling flow, i.e., $\beta > 0$ and constant, the transient response time of the concentration field scales with $1/\beta$. After the transient time passes ($t > 1/\beta$), the advection and diffusion terms are balanced. In this case, the interfacial scalar flux q can be calculated analytically as:

$$q = \sqrt{\frac{2\beta}{\pi \cdot Sc}} \cdot \Delta C \quad (8)$$

where, ΔC is a concentration difference between the interface and the bulk.

Conversely, if β is negative, i.e., in the case of flow away from the interface, the concentration boundary layer is stretched exponentially with time, so that the scalar flux rapidly diminishes. Hence, if the renewal time scale of $1/\omega$ is sufficiently larger than the transient time $1/\beta$, i.e., $\beta/\omega \gg 1$, the interfacial scalar flux is estimated as follows:

$$q = \begin{cases} \sqrt{\frac{2\beta}{\pi \cdot Sc}} \cdot \Delta C \cong 0.8 \sqrt{\frac{\beta}{Sc}} \cdot \Delta C & \beta > 0 \\ 0 & \beta < 0 \end{cases} \quad (9)$$

In Fig. 7, the gas transfer rate obtained by solving Eq. (7) is plotted as a function of β/ω . The correlation coefficient between the normal velocity and scalar fluctuations at the interface is also plotted. When $\beta/\omega > 1$, the correlation coefficient is quite high and the gas transfer rate is predicted fairly well by Eq. (5).

When $\beta/\omega < 1$, however, both the gas transfer rate and the correlation coefficient decrease drastically. In this case, the velocity fluctuates so frequently that the balance between the advection and diffusion terms does not hold near the interface anymore. Instead, the advection term balances with the time-derivative term in Eq. (7). Consequently, the velocity fluctuation is out of phase with the concentration fluctuation and hardly contributes to mass transfer.

According to these results, we can conclude that the velocity fluctuation which satisfies the condition $\beta/\omega > 1$ dominates the interfacial mass transfer. If this is the case, the local scalar flux should be predicted from the surface divergence by Eq. (9).

Time-series of the local scalar flux. Examples of time-series of the local scalar flux at $Sc_L = 1.0$ and 100 , the surface divergence and the prediction by Eq. (9) at clean and contaminated interfaces are shown in Figs. 8a and 8b, respectively. For $Sc_L = 1.0$, the difference of the concentration between the interface and $y^+_L = 20$, $\Delta C_{y^+=20}$ is used instead of ΔC in Eq. (9), since the concentration boundary layer extends outside of the viscous layer. At a clean interface, Eq. (9) predicts local peak values fairly well, indicating that the local scalar flux is determined by the balance between the normal advection and diffusion terms.

In Fig. 9, the contribution of surface divergence to the scalar flux is shown. The prediction by Eq. (9) is depicted as a solid line. At a clean interface, the scalar transfer mostly occurs when the surface dilates, i.e., $\beta > 0$ and PDF shows good agreement with Eq. (9) (see, Fig. 9a). With increasing the Marangoni number, however, the prediction by Eq. (9) becomes worse. Especially, at the highly contaminated case, it is obvious that the local scalar flux hardly responds to the surface divergence (see, Fig. 8b). This is a primary reason why the gas transfer rate is almost independent of the surface divergence at highly contaminated interfaces.

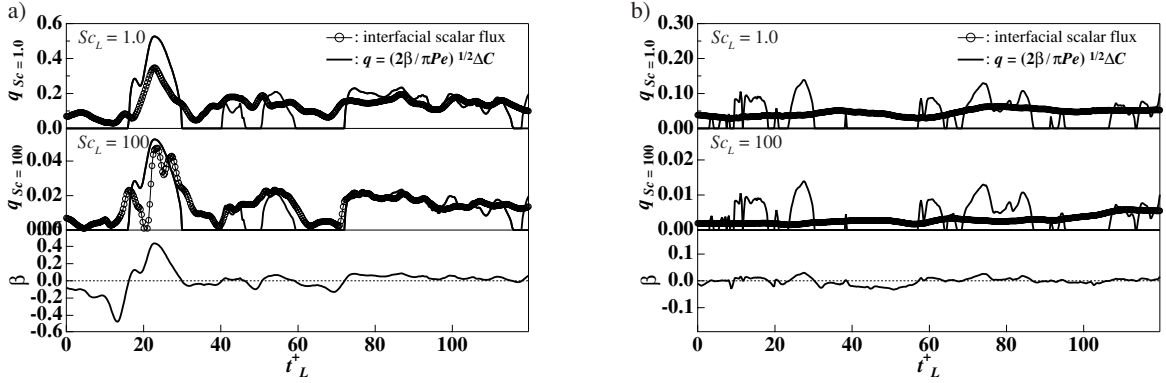


Figure 8: Time-series of the interfacial scalar flux q at $Sc_L = 1.0$ and 100, prediction by Eq. (9) and the surface divergence β in a): Clean and b): Case 2.

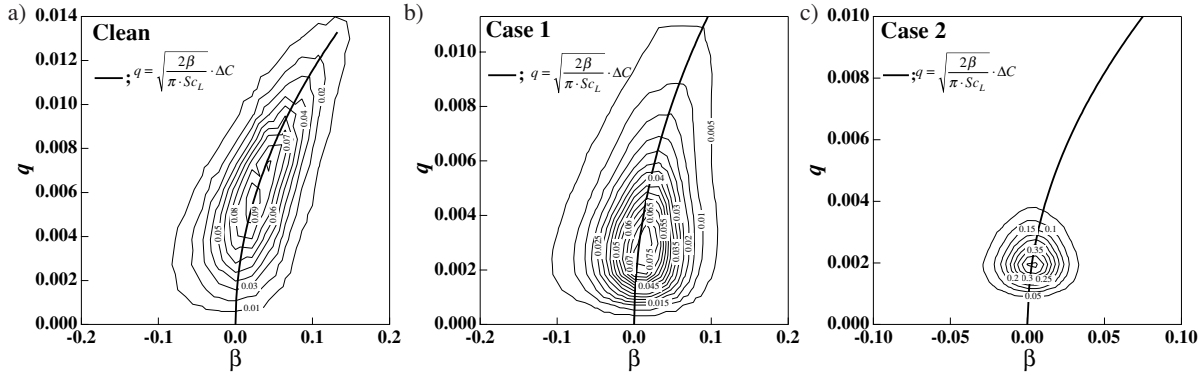


Figure 9: Contribution of the surface divergence β to the interfacial scalar flux q at $Sc_L = 100$ in a): Clean, b): Case 1 and c): Case 2. Solid line: prediction by Eq. (9).

Extraction of effective surface divergence. According to the analysis based on the one-dimensional advection-diffusion equation, the fluctuating surface divergence contributes to mass transfer only when its duration time $1/\omega$ is longer than its transient time $1/\beta$, i.e., $\beta/\omega > 1$. Hence, it is interesting to see the magnitude relationship between β and ω at clean and contaminated interfaces. However, it is not straightforward to define them, since a wide range of frequencies are present in real turbulent flows. Therefore, we made simple estimation as follows.

Suppose an ideal constant surface divergence β occurs (see, Fig. 10a), the time required to reach the steady solution given by Eq. (9) is $1/\beta$. In a similar way, in the case of turbulent flows, we extract the surface divergence between neighboring zero-crossing points (t_1 and t_2 in Fig. 10b) and calculate the following integral F :

$$F = \int_{t_1}^{t_2} \beta(t) dt \quad (10)$$

If $|F| > 1$, we deem that the interfacial scalar flux is given by Eq. (9). Otherwise, it is assumed that the surface divergence does not contribute to the mass transfer at all.

In Fig. 11, the contribution of β_c and ω_c to the total sur-

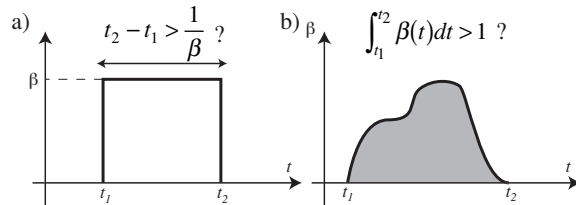


Figure 10: Extraction of effective surface divergence β_E in the case of a): constant β , and b) fluctuating β .

face divergence for the clean surface and Case 2 are shown. Here, the frequency ω_c is defined as $\omega_c = 2\pi/T_c$, where T_c is a period between the two neighboring zero-crossing points. The amplitude β_c is a mean of the surface divergence during the period. By definition, $\beta_c T_c = F$ and $F = 1$ and -1 are depicted as dotted lines.

At the clean interface, 90 % of the total power resides outside of the two lines, i.e., $|F| > 1$. With increasing the Marangoni number, the percentage decreases to 34%, 2% and 0% in Cases 1, 2 and 3, respectively. The typical trend of the contaminated interface appears as damping of β_c , while the peak frequency is almost unchanged, namely, $\omega_c \sim 0.3$

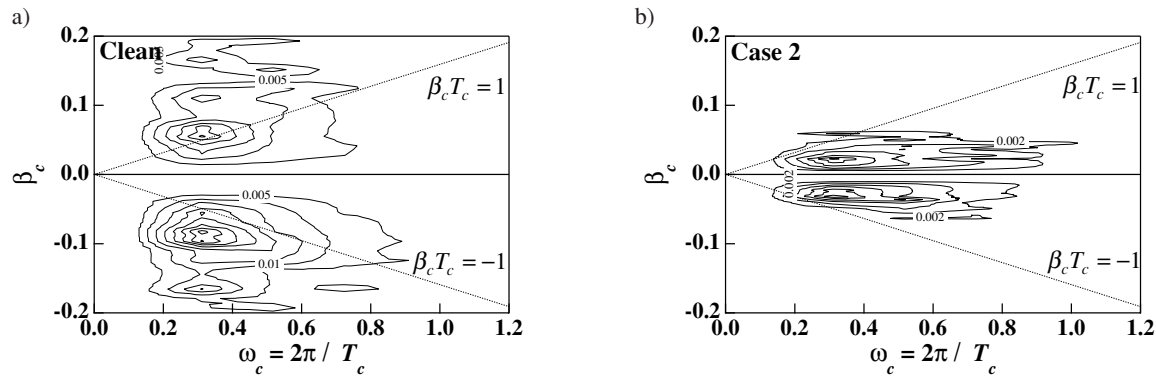


Figure 11: Contribution of β_c and ω_c to the total power of surface divergence in a): Clean and b): Case2.

or $T_c \sim 20$ in the shear units (see, Figs. 11a and 11b). This suggests that the transit time of a streamwise vortex outside of the viscous sublayer is hardly affected by the surface contamination.

From the power contained in the area of $|F| > 1$, we estimate the effective surface divergence $\beta_{E\text{rms}}$. The gas transfer rate is replotted against $\beta_{E\text{rms}}$ with solid symbols in Fig. 5. For the clean and slightly contaminated (Case 1) interfaces, the gas transfer rate is predicted fairly well from the effective surface divergence by Eq. (5). On the other hand, in the highly contaminated cases (Cases 2 and 3), the effective surface divergence is too small to explain the present data. Instead, the interface is more like a solid wall.

CONCLUSIONS

Numerical simulation of high Schmidt number turbulent mass transfer across clean and contaminated interfaces was carried out. At the clean interface, the Chan and Scriven's irrotational stagnation model given by Eq. (9) predicts the local scalar flux fairly well, indicating that an upwelling flow induced by the surface divergence is the essential mechanism of the interfacial mass transfer. This would be a primary reason why the surface divergence model is robust under a wide range of flow conditions.

With increasing the Marangoni number, however, the correlation between the local scalar flux and the surface divergence deteriorates drastically. Specifically, at highly contaminated interfaces, the gas transfer rate is almost independent of the surface divergence and converges to the value on a solid wall.

From an analysis of a one-dimensional advection-diffusion equation, it was shown that the surface divergence contributes to mass transfer only when the renewal time scaled by $1/\omega$ is larger than the transient time scaled by $1/\beta$, namely, $\beta/\omega > 1$.

The major effect of surface elasticity is damping of β ,

while ω is almost unchanged. This leads to strong attenuation of the effective surface divergence at the higher Marangoni numbers.

The intensity of the effective surface divergence was found suitable for prediction of gas exchange at clean and slightly contaminated interfaces. For a highly contaminated interface, in which the effective surface divergence is strongly damped, the mass transfer is essentially the same as that on a solid wall.

ACKNOWLEDGMENT

The present work was supported through the 21st Century COE Program, "Mechanical Systems Innovation," by the Ministry of Education, Culture, Sports, Science and Technology.

REFERENCES

- Asher, W., and Pankow, J. F., 1986, "The interaction of mechanically generated turbulence and interfacial films with a liquid phase controlled gas/liquid transport process", *Tellus*, Vol. 38B, pp. 305-318.
- Banerjee, S., Lakehal, D., and Fulgosi, M., 2004, "Surface Divergence Models for Scalar Exchange between Turbulent Streams", *Int. Journal of Multiphase Flow*, Vol. 30, pp. 963-977.
- Chan, W. C., and Scriven, L. E., 1970, "Absorption into Irrotational Stagnation Flow", *Ind. Engng Chem. Fundam.*, Vol. 9, No. 1, pp. 114-120.
- Jähne, B., Münnich, K. O., Böisinger, R., Dutzi, A. Huber, W., and Libner, P., 1987, "On the Parameters Influencing Air-Water Gas Exchange", *Journal of Geophysical Research*, Vol. 92, No. C2, pp. 1937-1949.
- McCready, M. J., Vassiliadou, E., and Hanratty, T. J., 1986, "Computer Simulation of Turbulent Mass Transfer at a Mobile Interface", *AIChE Journal*, Vol. 32, No. 7, pp. 1108-1115.